

Topology of Electronic Densities Taken from Parametric Methods: A Predictive Tool?

ANIBAL SIERRAALTA, FERNANDO RUETTE, ERICK MACHADO

Laboratorio de Química Computacional, Centro de Química, Instituto Venezolano de Investigaciones Científicas, Apartado 21827, Caracas 1020-A, Venezuela

Received 10 June 1997; revised 3 September 1997; accepted 4 September 1997

ABSTRACT: Calculations of topological properties of the Laplacian of the electronic density function [$-\nabla^2\rho(\mathbf{r})$] evaluated with a parametrical (CNDO) and full-electron ab initio HF methods were performed. Results for CH_4 , CH_3Cl , CCl_4 , H_2S , and PH_3 molecules show that the use of the symmetrical transformation to the basis set is adequate to build the CNDO electronic density functions that reproduce, in a qualitative way, the topology of $-\nabla^2\rho(\mathbf{r})$ obtained from full-electron ab initio calculations. The topology of $-\nabla^2\rho_{\text{spin}}(\mathbf{r})$ was evaluated using CNDO calculations. An analysis of the critical points was carried out on modeled catalysts (Ni_5 and $\text{Mo}_3\text{S}_{14}\text{H}_4$ clusters) to study the adsorption of C on Ni_5 and dissociation of H_2 on $\text{Mo}_3\text{S}_{14}\text{H}_4$. The location of critical points was associated with the most reactive sites on the cluster surface and used to predict the C adsorption path and the most convenient orientation of H_2 for dissociation. © 1998 John Wiley & Sons, Inc. *Int J Quant Chem* 70: 113–123, 1998

Introduction

The topological properties of the negative of the electronic density Laplacian $-\nabla^2\rho(\mathbf{r})$ [1] have become an important tool for the interpretation of results obtained from quantum chemistry calculations. Reactivity and catalytic active sites [2] can be characterized without a tedious analysis of

the molecular orbitals. The characterization can be done using only the topological properties of the electronic molecular density $\rho(\mathbf{r})$ and its Laplacian.

It is well known that ab initio calculations for transition-metal compounds are highly demanding in computing resources, even at the Hartree–Fock level, due to the great number of electronic integrals involved. Semiempirical and model Hamiltonian methods, by their own nature, reduce the computational costs considerably. These methods usually are parametrized in order to obtain a good agreement between the experimental and the calculated geometries and binding energies; never-

Correspondence to: A. Sierraalta.
Contract grant sponsor: CONICIT.
Contract grant number: S1-2690.

theless, it is not clear if the $\rho(\mathbf{r})$'s derived from these methods can be used in the analysis of the topological properties of $-\nabla^2\rho(\mathbf{r})$.

Previous work [3, 4] using model Hamiltonians with ab initio core potentials (ECP methodologies) have shown that the topological properties, such as geometrical locations of critical points CPs and their relative values, of $\rho(\mathbf{r})$ and $-\nabla^2\rho(\mathbf{r})$ in the bonding and valence regions are similar to those obtained by full-electron HF calculations. Edgecombe et al. [5] showed also that the semiempirical AM1 method reproduces the full-electron HF 6-31G results for the bond critical points.

Since there are numerous sites on a catalytic surface and different ways to orientate an adsorbate, the location of valence electronic charge concentrations and depletions in the adsorbate and on the surface can be very useful for the determination of the reaction pathway in catalytical processes. For example, the H_2 interaction with the sulfur atoms of small MoS_2 clusters (Mo_3S_6 and Mo_2S_6) was analyzed in a previous work [6]. Results showed that the maxima of $-\nabla^2\rho_{\text{spin}}(r)$ and not the maxima of $-\nabla^2\rho(r)$ give the correct answer for the H_2 -dissociation active sites. H_2 on MoS_2 is dissociated on sites that contain two neighbor S atoms, leading to the formation of two $-\text{SH}$ groups.

The aim of the present work was to show for the first time that it is possible to use the topological properties of electronic densities extracted from quantum chemical methods based on parametric functionals, such as the complete neglect differential overlap method (CNDO) to characterize the reactive sites of molecules and modeled catalysts. The CNDO method has been used to study some catalytic reactions [7–9].

Background

Bader and other authors [1, 2, 10–13] have shown that the analysis of the topology of the Laplacian of the molecular electronic density gives detailed information about the charge distribution and reactivity. The regions where the electronic charge is locally depleted are characterized by $-\nabla^2\rho(\mathbf{r}) < 0$, and those where charge is locally concentrated, by $-\nabla^2\rho(\mathbf{r}) > 0$. The critical points of $-\nabla^2\rho(\mathbf{r})$, i.e., the points where the gradient of $-\nabla^2\rho(\mathbf{r})$ is zero, are classified according to their type (λ, σ) . The rank (λ) is equal to the number of

nonzero eigenvalues of the Hessian matrix of $-\nabla^2\rho(\mathbf{r})$ evaluated at the critical points. The signature (σ) is the algebraic sum of the signs of the eigenvalues. Only four types of critical points are possible: $(3, -3)$, a local maximum; $(3, +3)$, a local minimum; and saddle points, $(3, -1)$ and $(3, +1)$.

According to Bader's theory [1], the reactive sites in a molecule are associated with the type and number of critical points of $-\nabla^2\rho(\mathbf{r})$ at the outer valence shell of charge concentration OVSCC. In an acid–base reaction, the largest $(3, -3)$ critical point of the base reacts with the deepest $(3, +1)$ critical point of the acid. For example, it has been shown [11a] that the active sites on O—Mg or O—Li for hydrogen abstraction from CH_4 correspond to the $(3, +1)$ critical points of the $-\nabla^2\rho(\mathbf{r})$.

Methodology

The calculations were performed using the HONDO-8 program of the MOTEC-90 package [14] and the modified semiempirical CNDO-UHF method from the GEOMO program [15]. The topological properties of $-\nabla^2\rho(\mathbf{r})$ were calculated with a modified version of the BUBBLE program [16, 17]. Full-electron ab initio HF calculations were carried out with the 6-31G [18] basis set. For Cl, P, and S atoms, the atomic basis set of the CNDO method include *d* atomic orbitals; therefore, *d* orbitals were also used in the full-electron calculations.

The single-zeta Slater-type atomic basis set of the CNDO library was used as the atomic basis to construct the semiempirical electronic density. The molecular orbitals that arise from semiempirical or parametric Hamiltonians are expressed in an orthogonal atomic basis set that is unknown, because in the SCF process of these methods, the overlap matrix is assumed to be diagonal. Three sets of molecular orbitals were employed to construct the electronic density functions. The first set was obtained from the final SCF-CNDO molecular orbitals, in which the nonorthogonalized single-zeta Slater-type atomic basis set was employed. For the second and third sets of molecular orbitals, symmetric and canonical orthogonalization are assumed; therefore, the final SCF-CNDO molecular orbitals are changed to the nonorthogonalized basis set, using the corresponding transformation matrix.

Results and Discussion

In this section, the topological properties of $-\nabla^2\rho(\mathbf{r})$ at the OVSCC of the atoms are analyzed (a) in CH_4 , CH_3Cl , CCl_4 , H_2S and PH_3 molecules; (b) for a Ni_5 cluster; (c) for C adsorption on Ni_5 ; and (d) for H_2 dissociation on a $\text{Mo}_3\text{S}_{14}\text{H}_4$ aggregate, by comparing the CNDO with the full-electron HF results.

TOPOLOGICAL PROPERTIES OF $-\nabla^2\rho(\mathbf{r})$ FOR MOLECULES

The values of the maxima of $-\nabla^2\rho(\mathbf{r})$ ($-\nabla^2\rho_{\text{max}}$) at the OVSCC region of the carbon atom and the distance from the nuclei to $-\nabla^2\rho_{\text{max}}$ ($R_{\text{C-cp}}$) using full-electron HF $\rho_{\text{FE}}(\mathbf{r})$ and CNDO electronic densities for CH_4 , CH_3Cl , and CCl_4 molecules are listed in Table I. The results show that the same spatial localization and number of maxima of $-\nabla^2\rho_{\text{FE}}(\mathbf{r})$ are also obtained with CNDO nontransformed and symmetrically transformed orbital densities. In the CCl_4 molecule, according to the full-electron results, the C atom has four equally and symmetri-

cally spaced $-\nabla^2\rho_{\text{max}}$ values. The CNDO densities show, however, a small spread in the values of $R_{\text{C-cp}}$ and $-\nabla^2\rho_{\text{max}}$. This spread may be due to the low quality of the semiempirical basis set (single-zeta) or to the use of a noncomplete appropriate orthogonal transformation. In the case of canonical orbital orthogonalization, a completely different picture was obtained. Two maxima, instead of four, appear in the OVSCC region of the C atom for all molecules.

The behavior observed in the topology of $-\nabla^2\rho(\mathbf{r})$ for the C atom (full electron vs. CNDO) was also found for the $-\nabla^2\rho(\mathbf{r})$ of the Cl, P, and S atoms in the CH_3Cl , CCl_4 , H_2S , and PH_3 molecules (see Table II). Again, there is a spread between the values for the symmetrically transformed case that does not appear in the full-electron results. For example, the $-\nabla^2\rho_{\text{FE}}(\mathbf{r})$ of the P atom in the PH_3 molecule presents three maxima of equal magnitude ($-\nabla^2\rho_{\text{max}} = 0.422$) in the regions of the P—H bonds and one of lower magnitude in the opposite region ($-\nabla^2\rho_{\text{max}} = 0.311$). The topology of the $-\nabla^2\rho(\mathbf{r})$ using the CNDO density, shows two maxima of equal magnitude ($-\nabla^2\rho_{\text{max}} = 0.328$) and one somewhat different ($-\nabla^2\rho_{\text{max}} = 0.292$) in the P—H bond regions. In

TABLE I
Topological properties of $-\nabla^2\rho(\mathbf{r})$ at the VSCC of the C atom.^a

	Full electron	Not orthogonalized	Symmetric	Canonical
Molecule: CH_4				
$R_{\text{C-cp}}$ (au)	0.980(4)	0.685(4)	0.686(4)	0.487(1) 0.479(1)
$-\nabla^2\rho_{\text{max}}$ (au)	0.834(4)	1.714(4)	1.064(4)	8.550(1) 8.592(1)
Molecule: CH_3Cl				
$R_{\text{C-cp}}$ (au)	0.956(3) 1.060(1)	0.670(3) 0.703(1)	0.679(3) 0.659(1)	0.464(1) 0.465(1)
$-\nabla^2\rho_{\text{max}}$ (au)	0.953(3) 0.279(1)	1.744(3) 1.254(1)	1.069(3) 0.995(1)	8.934(1) 7.324(1)
Molecule: CCl_4				
$R_{\text{C-cp}}$ (au)	0.978(4)	0.670(2) 0.674(1) 0.675(1)	0.653(2) 0.657(1) 0.656(1)	0.569(1) 0.568(1)
$-\nabla^2\rho_{\text{max}}$ (au)	0.600	1.413(2) 1.397(1) 1.423(1)	1.032(2) 1.038(1) 1.023(1)	3.167(1) 2.568(1)

^aNo. in parentheses means the no. of maximas of equal value.

TABLE II
Topological properties of $-\nabla^2\rho(\mathbf{r})$ at the VSCC of the Cl, P, and S atoms for CH_3Cl , CCl_4 , PH_3 , and H_2S molecules.^a

	Full electron	Not orthogonalized	Symmetric	Canonical
<u>Molecule: CH_3Cl (Cl atom)</u>				
$R_{\text{Cl-cp}}$ (au)	1.171(3) 1.262(1)	0.930(2) 0.950(1)	0.941(2) 0.949(1) 1.017(1)	5 critical points
$-\nabla^2\rho_{\text{max}}$ (au)	0.853(3) 0.614(1)	1.845(2) 2.031(1)	1.664(2) 1.524(1) 0.947(1)	
<u>Molecule: CCl_4 (Cl atom)</u>				
$R_{\text{Cl-cp}}$ (au)	1.167(3) 1.281(1)	0.929(2) 0.946(1) 0.961(1)	0.941(2) 0.948(1) 1.058(1)	6 critical points
$-\nabla^2\rho_{\text{max}}$ (au)	0.899(3) 0.561(1)	1.864(2) 1.547(1) 1.827(1)	1.660(2) 1.540(1) 0.697(1)	
<u>Molecule: PH_3 (P atom)</u>				
$R_{\text{Cl-cp}}$ (au)	1.617(3) 1.439(1)	1.204(2) 1.229(1) 1.167(1)	1.269(2) 1.286(1) 1.204(1)	0.644(1) 0.884(1) 0.993(1) 1.043(1)
$-\nabla^2\rho_{\text{max}}$ (au)	0.422(3) 0.311(1)	0.878(2) 0.762(1) 0.492(1)	0.328(2) 0.292(1) 0.389(1)	0.366(1) 0.824(1) 1.974(1) 1.645(1)
<u>Molecule: H_2S (S atom)</u>				
$R_{\text{Cl-cp}}$ (au)	1.290(2) 1.404(2)	1.010(2) 1.107(2)	1.027(2) 1.184(2)	6 critical points
$-\nabla^2\rho_{\text{max}}$ (au)	0.576(2) 0.496(2)	1.352(2) 0.971(2)	1.107(2) 0.416(2)	

^aNo. in parentheses means no. of maximas of equal value.

addition, the maximum of higher magnitude is located in the opposite region ($-\nabla^2\rho_{\text{max}} = 0.389$), contrary to the full-electron results.

The CNDO's orbitals transformed canonically give a distinct number of maximas of $-\nabla^2\rho$ with different spatial directions than those obtained with FE densities. For example, when the canonical transformation is used, the OVSCC of the S atom in the H_2S molecule presents six maximas instead of the four that appear in the full-electron case. For all molecules studied here, the symmetric transformation of the CNDO orbitals produces $\rho(\mathbf{r})$ and $-\nabla^2\rho(\mathbf{r})$ whose topological properties (type, number, and spatial locations of critical points) are qualitatively correct. The nontransformed CNDO orbitals reproduces in most of the cases the full-

electron picture, except for Cl in the CH_3Cl molecules where three maximas (two $-\nabla^2\rho_{\text{max}} = 1.845$ and one $-\nabla^2\rho_{\text{max}} = 2.031$) instead of four were observed.

The CNDO densities produce higher values of $-\nabla^2\rho_{\text{max}}$ and shorter distances $R_{A\text{-cp}}$ than those obtained with the full-electron densities. These features are characteristic of the only valence-electron densities [6] and are a consequence of the absence of the core electrons. The core electronic density not only pushes out the valence one by the electron-electron repulsion effect and by the shielding of the nuclear charge, i.e., by the dynamic interaction between core electrons and valence ones (radial correlation), but also makes an important contribution to the OVSCC of the atoms. As a

matter of fact, full-electron densities, where the core electron molecular orbitals are removed by hand, present behavior similar to the only-valence-electron densities such as lower $R_{\text{atom-cp}}$ and higher $-\nabla^2\rho_{\text{max}}$ values than those of the corresponding all-electron ones [6]. These results show the convenience of using the symmetric transformation in parametric Hamiltonians in order to produce electronic densities that qualitatively give the same topology as that of all-electron calculations.

VALENCE SHELL CHARGE CONCENTRATIONS ON Ni ATOMS OF A Ni₅ CLUSTER

Previous works using MINDO/SR methodology [19, 20] have shown that one carbon atom can be adsorbed into the surface of a square-base pyramidal Ni₅(4,1) cluster. We performed here calculations for this cluster with a spin multiplicity of 5 and 7 and for Ni₅—C systems with a multiplicity

of 3, but using the CNDO method. According to the results obtained in the previous section, only the symmetrically transformed orbitals are used, because their derived densities have a qualitatively correct topology. In addition, this type of transformation is able to give very reasonable Mulliken populations on metallic atoms [21]. Beside this, the not-transformed orbitals usually give wrong charges on the metals [7]. We also analyzed the topology of the Laplacian of the spin density $-\nabla^2\rho_{\text{spin}}(\mathbf{r})$. The spin density $\rho_{\text{spin}}(\mathbf{r})$ is calculated as the difference between the electronic density corresponding to alpha electrons $\rho_{\alpha}(\mathbf{r})$ minus the electronic density for beta electrons $\rho_{\beta}(\mathbf{r})$ [$\rho_{\text{spin}}(\mathbf{r}) = \rho_{\alpha}(\mathbf{r}) - \rho_{\beta}(\mathbf{r})$].

The values of $R_{\text{Ni-cp}}$ and $-\nabla^2\rho_{\text{max}}$ at the OVSCC of the Ni atoms are reported in Table III. Starting with different electronic configurations for the initial guess core Hamiltonian, two electronic states (7-I and 7-II) were found for the septuplet electronic state of the Ni₅(4,1) cluster. The electronic

TABLE III
Topological properties of $-\nabla^2\rho(\mathbf{r})$ and $\nabla^2\rho_{\text{spin}}(\mathbf{r})$ at the VSCC of the Ni atoms in a Ni₅ cluster.^a

Electronic state	ΔE (kcal/mol)	Ni atom	$R_{\text{Ni-cp}}$ (au)	$-\nabla^2\rho_{\text{max}}$ (au)	Net charge	
7-I	0.00	1, 2, 4	0.380(2)	254.9	0.00	
			0.385(2)	234.3		
			0.381(2)	443.5		
		3	0.385(2)	210.2		0.00
			0.402(2)	152.1		
			0.401(2)	212.0		
5	0.404(4)	130.6	0.00			
	0.382(2)	548.9				
	0.380(2)	241.8				
7-II	+244.9	1, 2, 3, 4		0.387(2)	218.2	0.01
				0.385(2)	378.7	
				0.404(4)	130.6	
		5	0.328(2)	549.0	-0.04	
			0.366(2)	86.9		
			0.360(2)	221.2		
3	0.258(2)	69.7	0.00			
	0.312(2)	123.3				
	0.326(2)	117.0				
7-II	+244.9	1, 2, 3, 4		0.360(2)	86.4	+1.52
				0.359(2)	173.0	

^aNo. in parentheses means no. of maximas of equal value.

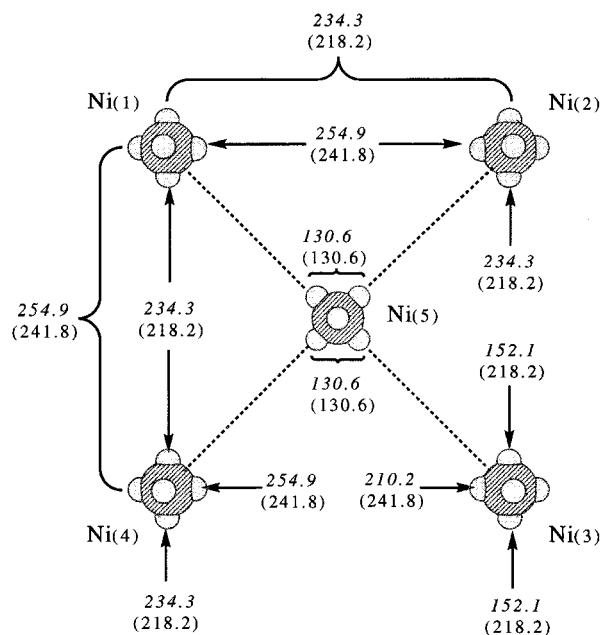


FIGURE 1. Schematic representation of the square-base pyramidal $Ni_5(4,1)$ cluster showing the position of the Ni atoms and of the $-\nabla^2\rho(\mathbf{r})_{\max}$ (small gray spheres). Italic numbers correspond to the 7-I electronic state. Nos. in parentheses correspond to the state 7-II.

state 7-II is 244.9 kcal/mol higher in energy than is the electronic state 7-I. For both states, the Ni atoms present an octahedral distribution of maxima of $-\nabla^2\rho(\mathbf{r})$ as displayed in Figure 1. Even though all the surface atoms [Ni(1), Ni(2), Ni(3), and Ni(4)] are equal by geometry, the state 7-I exhibits an asymmetry in the distribution of the local charge concentrations. The $-\nabla^2\rho_{\max}$ values for the Ni(3) atom are different from those obtained for the Ni(1), Ni(2), and Ni(4) atoms. This asymmetry is reflected more strongly in the atomic spin population and in the maxima of $-\nabla^2\rho_{\text{spin}}(\mathbf{r})$ [$-\nabla^2\rho(\text{spin})_{\max}$], where the Ni(3) atom has three different pairs of maxima, whereas the others only have two, as displayed in Figures 2 and 3. These results show that a spin polarization exists for the electronic state 7-I. This symmetry breaking may be due to the use of single determinant as a variational trial function or to the fact that 7-I corresponds to an excited electronic state.

For both states 7-I and 7-II, the maxima of $-\nabla^2\rho_{\text{spin}}(\mathbf{r})$ for the Ni(5) atom were not found. This shows that the local spin concentrations are highly localized over the top layer of surface Ni atoms. In general, the magnitude of the maxima of

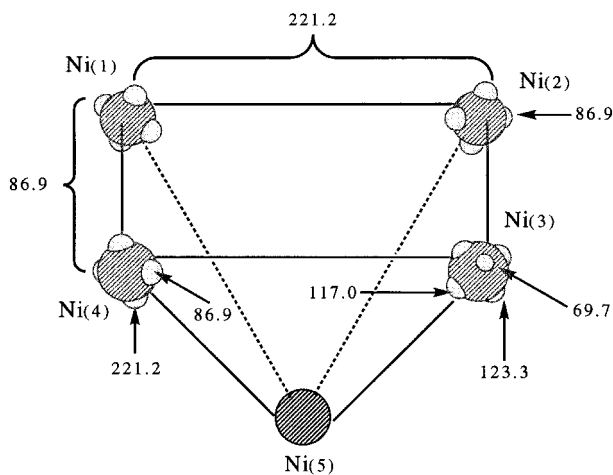


FIGURE 2. Schematic representation of the $Ni_5(4,1)$ cluster showing the position of the Ni atoms and of the $-\nabla^2\rho(\text{spin})_{\max}$ (small gray spheres) for the electronic state 7-I. Nos. correspond to $-\nabla^2\rho(\text{spin})_{\max}$ values. See Table III.

$-\nabla^2\rho(\text{spin})_{\max}$ are lower than that corresponding to $-\nabla^2\rho_{\max}$, because $\rho_{\text{spin}}(\mathbf{r})$ is associated with a lower number of electrons than that of the total molecular electronic density [$\rho(\mathbf{r})$].

Table IV displays the values of R_{Ni-cp} , $-\nabla^2\rho_{\max}$, and the net charge of the Ni atoms for the quintuplet electronic states. As in the case of the septuplet, two electronic states were found. The electronic state 5-II, which is higher in energy by

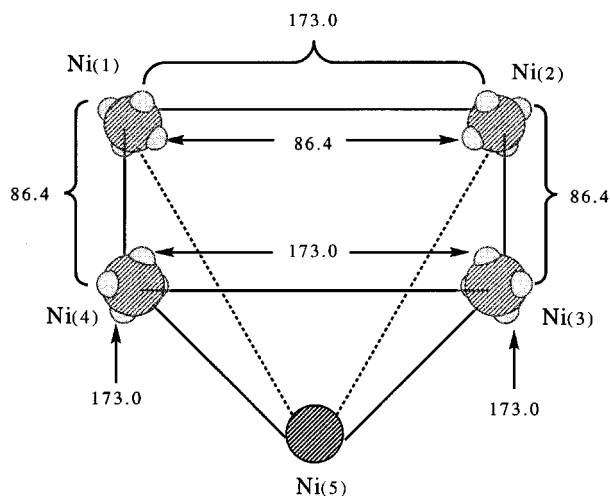


FIGURE 3. Schematic representation of the $Ni_5(4,1)$ cluster showing the position of the Ni atoms and of the $-\nabla^2\rho(\text{spin})_{\max}$ (small gray spheres) for the electronic state 7-II. Nos. correspond to $-\nabla^2\rho(\text{spin})_{\max}$ values. See Table III.

TABLE IV
Topological properties of $-\nabla^2\rho(\mathbf{r})$ at the VSCC
of the Ni atoms in a Ni₅ cluster.^a

Electronic state	ΔE (kcal/mol)	Ni atom	$R_{\text{Ni-cp}}$ (au)	$-\nabla^2\rho_{\text{max}}$ (au)	Net charge
5-I	0.00	1	0.376(2)	480.0	0.00
			0.378(2)	263.3	
			0.384(2)	241.2	
		2, 4	0.381(2)	442.3	0.00
			0.382(2)	245.0	
			0.384(2)	243.2	
		3	0.378(2)	458.8	0.00
			0.380(2)	256.6	
			0.384(2)	236.5	
		5	0.382(2)	548.9	0.00
0.404(4)	130.2				
5-II	+201.4	1, 2	0.380(2)	254.0	0.01
			0.381(2)	448.2	
			0.385(2)	234.4	
		3, 4	0.380(2)	253.3	0.02
			0.381(2)	445.7	
			0.385(2)	234.0	
		5	0.382(2)	549.0	-0.06
			0.400(4)	164.8	

^aNo. in parentheses mean no. of maximas of equal value.

+201.4 kcal/mol than the 5-I one, presents one small spread between the values of $-\nabla^2\rho_{\text{max}}$ for the set of atoms 1,2 and 3,4. As discussed in the previous section, this spread may be due to the quality of the basis set used and the use of a single-determinant wave function. Again, the lower-energy electronic state (state 5-I) has an asymmetric distribution of the OVSCC. This asymmetry is reflected in the spin density (see Table V) which shows not only that the maximum of spin population is localized over the Ni atoms 2 and 4, but also that the number of maxima of $-\nabla^2\rho_{\text{spin}}(\mathbf{r})$ is different for both electronic states 5-I and 5-II (see Figs. 4 and 5).

For the four electronic states found in this work, the order in energy, in respect to the most stable electronic state 5-I, is as follows: 5-I(0.00) < 7-I(+0.4) < 5-II(+201.4) < 7-II(+245.3) kcal/mol. Even though the electronic state 7-I is only +0.4 kcal/mol higher in energy than is state 5-I, their topologies of $-\nabla^2\rho_{\text{spin}}(\mathbf{r})$ are quite different. These results show that Laplacian density topology can be used to characterize different states, even those that are very close in energy.

CARBON ADSORPTION ON Ni₅ CLUSTER

One of the most important challenges in the topological theory of the electronic density is to predict a priori the reactive sites for a given reaction. This has been done frequently using the topological properties of $-\nabla^2\rho(\mathbf{r})$ [1] but also can be done using the local spin concentrations [6].

At the restricted open-shell HF level ROHF, when the spin multiplicity is different from 1, $\rho_{\text{spin}}(\mathbf{r})$ is associated with the higher-energy electrons; i.e., with the HOMO orbitals. Then, $-\nabla^2\rho_{\text{spin}}(\mathbf{r})_{\text{max}}$ must show the local charge concentration of the frontier electrons that are involved in the chemical reactions and, therefore, the location of the active sites.

At the UHF level, the situation could be different: The cancellation of the electronic density of the nonreactive beta electrons with the corresponding alpha ones could be incomplete. As far as the cancellation differs from zero, maxima in $-\nabla^2\rho_{\text{spin}}(\mathbf{r})$, related to the nonreactive electrons (tightly bound electrons), can appear. Besides this, for some electronic states, the set of frontier electrons could be composed of alpha as well as of beta electrons. In these cases, according to the definition of $\rho_{\text{spin}}(\mathbf{r})$, not only the maxima or the (3, -3) critical points of $-\nabla^2\rho_{\text{spin}}(\mathbf{r})$ are expected to correlate with the reaction sites, but also the (3, +3) CPs or minima of $-\nabla^2\rho_{\text{spin}}(\mathbf{r})$.

To investigate the relation between the (3, -3) critical points of $-\nabla^2\rho_{\text{spin}}(\mathbf{r})$ and the active sites, the adsorption of one C atom over a Ni₅(4,1) cluster was studied on four-center (FC), two-center (TC), and one-center (OC). Only the position of the C atom was optimized, and no relaxation of the cluster was done. According to our results, the adsorption occurs preferentially on the FC site following by the adsorption on TC, with the OC site being the less favored one.

Since the initial electronic state of the cluster can change due to the interaction with the C atom, calculations of the Ni₅(4,1)-C system with the C atom at a distance of 10 Å were performed. This calculation shows that the initial reactive state for the Ni₅(4,1) cluster corresponds to the electronic state 5-I. Figure 6 exhibits a schematic representation of the three final equilibrium positions of the C on the adsorption sites and the local spin concentrations of the electronic state 5-I of the Ni cluster. The FC adsorption takes place in the direction of the maxima of the highest magnitude of the Ni atoms (see Fig. 5). In this position, the C atom

TABLE V
Topological properties of $-\nabla^2\rho_{\text{spin}}(\mathbf{r})$ at the VSCC of the Ni atoms in a Ni_5 cluster.^a

Electronic state	ΔE (kcal/mol)	Ni atom	$R_{\text{Ni-cp}}$ (au)	$-\nabla^2\rho_{\text{spin}}(\mathbf{r})_{\text{max}}$ (au)	Spin population
5-I	0.00	1	0.265(2)	76.7	0.00
			0.272(2)	116.0	
			0.313(2)	146.5	
		2, 4	0.356(2)	44.2	2.00
			0.358(2)	220.7	
			0.366(2)	91.1	
		3	0.261(2)	80.5	0.00
			0.273(2)	121.3	
			0.311(2)	149.0	
		5	0.292(4)	1.2	0.00
0.353(2)	1.5				
5-II	+201.4	1, 2, 3, 4	0.360(2)	218.4	1.52
			0.364(2)	87.7	
		5	—	—	-2.07

^aNo. in parentheses means no. of maximas of equal value.

can interact with four local spin concentrations. For the OC site, the less reactive one, the C atom can interact only with one local spin concentration and its final equilibrium position coincides with the direction of one of the maximas of $-\nabla^2\rho_{\text{spin}}(\mathbf{r})$ of the Ni atom. Similarly, the equilibrium position of the C atom for the TC adsorption is located in the direction of two $-\nabla^2\rho_{\text{spin}}(\mathbf{r})_{\text{max}}$ CPs that belong to two Ni atoms, as displayed in Figure 6.

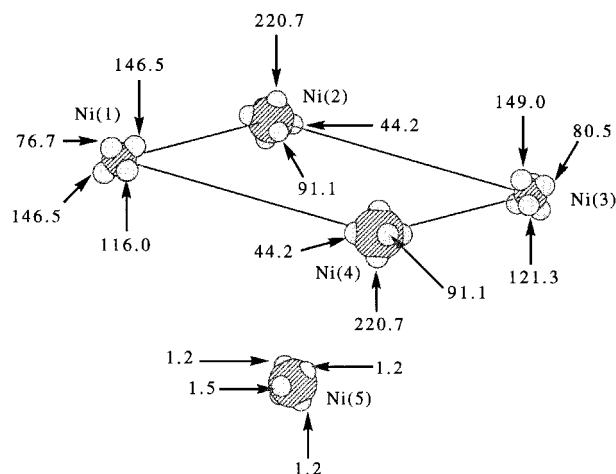


FIGURE 4. Schematic representation of the $\text{Ni}_5(4,1)$ cluster showing the position of the Ni atoms and of the $-\nabla^2\rho_{\text{spin}}(\mathbf{r})_{\text{max}}$ (small gray spheres) for the electronic state 5-I. Nos. correspond to $-\nabla^2\rho_{\text{spin}}(\mathbf{r})_{\text{max}}$ values. See Table V.

The above-mentioned results show that it is possible to predict qualitatively, by using the $-\nabla^2\rho_{\text{spin}}(\mathbf{r})$, the final geometry of one atom that interacts with a catalytic surface, provided that the reactive electronic state is known. For some cases, the interaction can be so strong that it changes the initial electronic state of the modeled catalytic surface. In these cases, the reactive site is not the

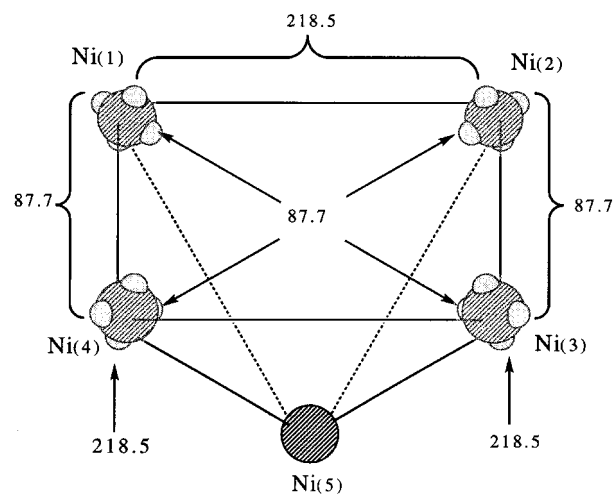


FIGURE 5. Schematic representation of the $\text{Ni}_5(4,1)$ cluster showing the position of the Ni atoms and of the $-\nabla^2\rho_{\text{spin}}(\mathbf{r})_{\text{max}}$ (small gray spheres) for the electronic state 5-II. Nos. correspond to $-\nabla^2\rho_{\text{spin}}(\mathbf{r})_{\text{max}}$ values. See Table V.

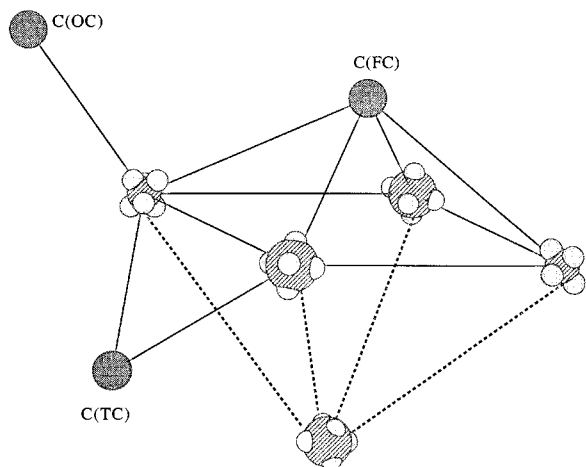


FIGURE 6. Schematic representation of the $\text{Ni}_5(4,1)$ cluster showing the equilibrium position of the C atom and of the $-\nabla^2\rho(\text{spin})_{\text{max}}$ (small gray spheres) for the FC, TC, and OC adsorption sites.

ground state but an excited one. Therefore, the Laplacian of the spin density of excited states must be analyzed.

H_2 DISSOCIATION ON A $\text{Mo}_3\text{S}_{14}\text{H}_4$ AGGREGATE

Molybdenum sulfide is a well-known catalyst used in the hydrodesulfuration processes. This catalyst reacts with the H_2 molecule to produce an anionic vacancy on the metallic atoms. The details of the mechanism are not known yet, in spite of the importance of this surface reaction [22]. Relatively little theoretical work has been done in this area [6, 23]. Nevertheless, it is well known that the H_2 molecule is dissociated by this catalyst. The aim of this section was to show that the analysis of the topology of $-\nabla^2\rho_{\text{spin}}(\mathbf{r})$, using the symmetrically transformed semiempirical densities, can be used to shed some light on the dissociative processes of H_2 on MoS_2 . The catalyst was modeled here by a molecular aggregate of $\text{Mo}_3\text{S}_{14}\text{H}_4$.

All the calculations were done at the UHF level using the CNDO method. For the S atom, a β value of 27.225 eV and the core integral values of 17.6469, 6.989, and 0.71325 eV for the 3s, 3p, and 3d orbitals were used. For the Mo atom $\beta(5s) = 7.500$, $\beta(5p) = 7.500$, and $\beta(4d) = 11.50$ eV, and the corresponding core integrals for the 5s, 5p, and 4d orbitals (3.930, 0.710, and 1.530 eV) were employed.

Figure 7 shows the molecular geometry of the $\text{Mo}_3\text{S}_{14}\text{H}_4$ aggregate and the position of maxima

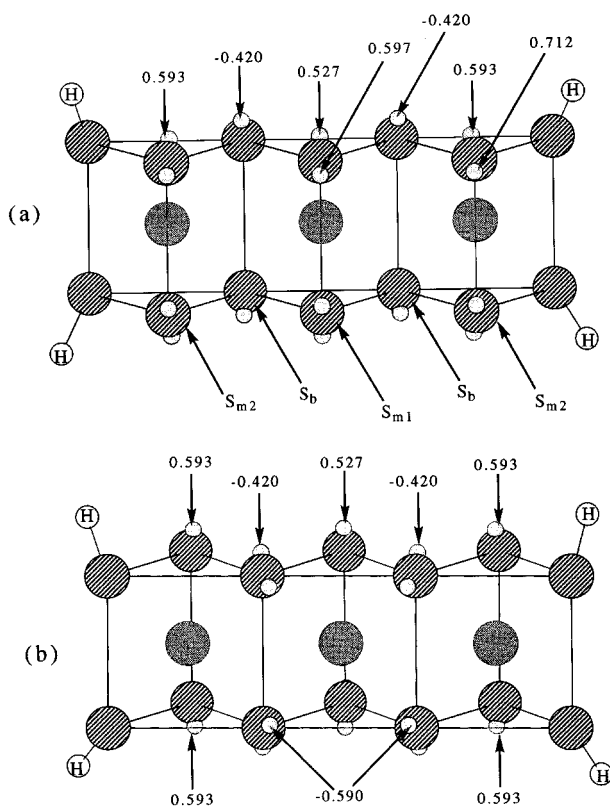


FIGURE 7. Schematic representation of the $\text{Mo}_3\text{S}_{14}\text{H}_4$ showing the positions of $-\nabla^2\rho(\text{spin})_{\text{max}}$ (small gray spheres) on S_{m1} , S_{m2} , and S_b atoms. Nos. correspond to $-\nabla^2\rho(\text{spin})_{\text{max}}$ values. (a) Front face. (b) Back face. See Table VI.

and minima of $-\nabla^2\rho_{\text{spin}}(\mathbf{r})$ at the valence shell of the S atoms. The $-\nabla^2\rho_{\text{spin}}(\mathbf{r})$ for the S_{m1} atom shows two maxima that correspond to (3, -3) CPs. One lies in the front face of the $\text{Mo}_3\text{S}_{14}\text{H}_4$ aggregate and whose value [$-\nabla^2\rho_{\text{spin}}(\mathbf{r}) = 0.597$ au] is greater than the other one [$-\nabla^2\rho_{\text{spin}}(\mathbf{r}) = 0.527$ au] that faces inside the aggregate. The $-\nabla^2\rho_{\text{spin}}(\mathbf{r})$ of the S_{m2} atoms presents two maxima whose magnitudes are greater than the corresponding ones in the S_{m1} atoms [see Fig. 7(a) and (b)].

The values of $-\nabla^2\rho_{\text{spin}}(\mathbf{r})$ at the critical points of the sulfur valence shell, the distances of the S nuclei to the critical points $R_{S\text{-cp}}$, the spin population, and the net charge are reported in Table VI. The S_{m1} atoms have a greater spin population than, and similar net charge to, the S_{m2} atoms. However, this is not correlated with the corresponding maxima of the local spin concentration. For example, the S_{m1} and S_{m2} atoms present spin populations of 1.43 and 0.50, respectively; however, the corresponding two maxima of $-\nabla^2\rho_{\text{spin}}(\mathbf{r})$

TABLE VI
Topological properties of $-\nabla^2\rho$ spin(\mathbf{r}) at the VSCC of S atoms in a molecular aggregated of $\text{Mo}_3\text{S}_{14}\text{H}_4$.^a

S atom	CP type	$R_{\text{S-cp}}$ (au)	$-\nabla^2\rho(\text{spin})_{\text{max}}$ (au)	Spin population	Net charge
S_b	(3, +3)	0.931(2)	-0.590(1)	-0.60	-0.13
		0.944(1)	-0.420(1)		
S_{m1}	(3, -3)	0.965(1)	0.597(1)	1.43	-0.08
		0.970(1)	0.527(1)		
S_{m2}	(3, -3)	0.907(1)	0.721(1)	0.50	-0.18
		0.922(1)	0.593(1)		

^aNo. in parentheses means no. of maximas of equal value.

exhibit average values of 0.58 and 0.66 au, respectively. The spin densities around these maxima are very reactive since they come from the highest occupied molecular orbitals, which in open-shell systems correspond to unpaired electrons. These high-energy electrons are able to interact with the antibonding σ^* orbital of the H_2 molecule to dissociate it. The geometrical disposition of the maxima of $-\nabla^2\rho_{\text{spin}}(\mathbf{r})$ indicates that the most probable dissociation path involves two maxima of $-\nabla^2\rho_{\text{spin}}(\mathbf{r})$ belonging to two S_{m1} or S_{m2} atoms. Our calculations show that, in fact, H_2 is dissociated by two neighbor S_{m1} or S_{m2} atoms when it is approximated by the $\text{Mo}_3\text{S}_{14}\text{H}_4$ aggregate in the direction of the two maxima of $-\nabla^2\rho_{\text{spin}}(\mathbf{r})$.

For open-shell RHF, the function $\rho_{\text{spin}}(\mathbf{r})$ is always greater or equal to zero, but in open-shell UHF, there is not an exact cancellation of $\rho_\alpha(\mathbf{r})$ with $\rho_\beta(\mathbf{r})$; therefore, $\rho_{\text{spin}}(\mathbf{r})$ can be positive or negative. Besides this, the set of HOMOs can be composed of alpha electrons as well as of beta electrons. Then, not only do the maxima of $-\nabla^2\rho_{\text{spin}}(\mathbf{r})$ indicate the possible active sites, but also the minima or (3, +3) CPs, which are related with the surplus of beta electrons over the alpha ones.

For the S_b -type sulfur atoms (see Fig. 7), the function $-\nabla^2\rho_{\text{spin}}(\mathbf{r})$ exhibits two (3, +3) critical points or minima instead of two maxima. As in the previous cases, the H_2 molecule is dissociated by two neighbor S_b atoms when the approaching is done in the direction of the (3, +3) CPs. The final position of the H atoms and the initial distribution of the critical points of $-\nabla^2\rho_{\text{spin}}(\mathbf{r})$ are displayed in Figure 8. Similar results were obtained for the modeling of H_2 dissociation on Mo_3S_6 and Mo_2S_6 clusters using the ab initio semicore effective core potential with an expanded basis set [6].

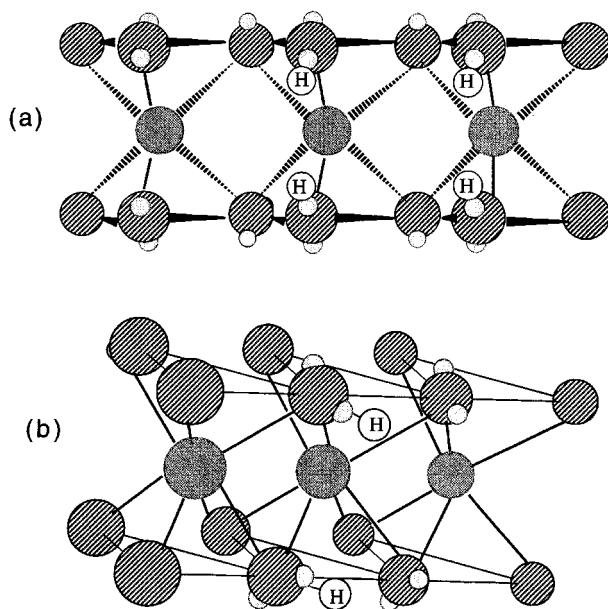


FIGURE 8. Schematic representation of the $\text{Mo}_3\text{S}_{14}\text{H}_4$ showing the positions of $-\nabla^2\rho(\text{spin})_{\text{max}}$ (small gray spheres) and the final positions of the H_2 dissociated. The H atoms corresponding to the $\text{Mo}_3\text{S}_{14}\text{H}_4$ are not shown.

Conclusions

The application of Bader's theory using parametrical methods such as CNDO has proved, for the first time, that it is possible to obtain valuable information with respect to the reactivity, analyzing the critical point of $-\nabla^2\rho(\mathbf{r})$ at the valence region. It is necessary, however, to transform the semiempirical molecular orbitals back to a nonorthogonal basis set by using a symmetric

transformation. Good qualitative topological properties of the $-\nabla^2\rho(\mathbf{r})$ (type and number of critical points and their spatial orientations), with respect to full-electron ab initio HF calculations, were found. The topology of $-\nabla^2\rho_{\text{spin}}(\mathbf{r})$, using densities from CNDO, can be also employed for the evaluation of chemical reactivity of active sites on catalysts. For example, it is possible to predict correctly the active sites for C adsorption on a Ni₅ cluster and for H₂ dissociation on a Mo₃S₁₄H₄ aggregate.

Due to that the semiempirical methods are parametrized with respect to geometries and/or experimental binding energies and not with respect to the electronic density, we expect that not all parametric methods can give reasonable electronic densities. Studies with other parametric methods are in progress.

ACKNOWLEDGMENTS

The authors want to acknowledge the contribution of CONICIT for providing an IBM-RISC 6000 Model-3BT workstation (Project S1-2690) and financial support to E. M. We also thank to CYTED V-4 and RED TEMATICA: Química Computacional for allowing the discussion and diffusion of these results and Dr. Juan Rivero for revising our manuscript.

References

1. R. F. W. Bader, *Atoms in Molecules: a Quantum Theory* (Clarendon Press, Oxford, 1990).
2. R. F. W. Bader, *Chem. Rev.* **91**, 893 (1991).
3. A. Sierralta and F. Ruetter, *J. Comp. Chem.* **15**, 313 (1994).
4. A. Sierralta and F. Ruetter, *Int. J. Quantum Chem.* **60**, 1015 (1996).
5. M. Ho, H. Schmider, K. E. Edgecombe, and V. D. Smith, *Int. J. Quantum Chem.* **S28**, 215 (1994).
6. A. Sierralta and F. Ruetter, *J. Mol. Catal.* **109**, 227 (1996).
7. A. E. Gainza, E. N. Rodríguez-Arias, and F. Ruetter, *J. Mol. Catal.* **85**, 345 (1993).
8. F. Ruetter and E. V. Ludeña, *J. Mol. Catal.* **67**, 266 (1981).
9. F. Ruetter, N. Valencia, and R. Sanchés-Delgado, *J. Am. Chem. Soc.* **111**, 40 (1989).
10. (a) R. F. W. Bader, R. J. Gillespie, and P. J. MacDougall, *J. Am. Chem. Soc.* **110**, 7329 (1988). (b) R. J. Gillespie, *Can. J. Chem.* **70**, 742 (1992). (c) P. J. MacDougall, M. B. Hall, R. F. W. Bader, and J. R. Cheeseman, *Can. J. Chem.* **67**, 1842 (1989). (d) R. F. W. Bader, P. L. A. Popelier, and C. J. Chang, *J. Mol. Struct. (Theochem)* **255**, 145 (1992).
11. (a) Y. Aray, J. Rodríguez, J. Murgich, and F. Ruetter, *J. Phys. Chem.* **97**, 8393 (1993). (b) Y. Aray, F. Rosillo, and J. Murgich, *J. Am. Chem. Soc.* **116**, 10639 (1994).
12. Y. Aray and J. Rodríguez, *Can. J. Chem.* **74**, 1014 (1996).
13. Y. Aray and R. F. W. Bader, *Surf. Sci.* **351**, 233 (1996).
14. MOTECC-90TM (IBM Corporation Center for Scientific and Engineering Computation, Kingston, NY, 1990).
15. (a) D. Rinaldi, P. E. Hoggan, and A. Cartier, GEOMO Program, QCPE, No. 290. (b) A. J. Hernández, F. Ruetter, and E. V. Ludeña, *J. Mol. Catal.* **39**, 21 (1987).
16. P. Krugg and R. F. W. Bader, private communication (Department of Chemistry, McMaster University, Hamilton, Ontario, 1990).
17. Y. Aray, J. Rodríguez, and R. López-Boada, *J. Phys. Chem.* **101**, 2178 (1997).
18. (a) R. Ditchfield, W. J. Hehre, and J. A. Pople, *J. Chem. Phys.* **54**, 724 (1971); (b) W. J. Hehre, R. Ditchfield, and J. A. Pople, *J. Chem. Phys.* **56**, 2257 (1972).
19. F. P. Poveda, A. Sierralta, J. L. Villaveces, and F. Ruetter, *J. Mol. Catal.* **106**, 109 (1996).
20. F. Ruetter and F. M. Poveda, in *Electronic Processes at Solid Surfaces*, E. Ilicsa and K. Makoshi, Eds. (World Scientific, Singapore, 1996), p. 303.
21. R. Atencio, L. Rincón, R. Sánchez-Delgado, and F. Ruetter, *J. Mol. Catal.*, submitted.
22. F. E. Massoth and P. Zeuthen, *J. Catal.* **145**, 216 (1994).
23. (a) A. B. Anderson, Z. Y. Al-Saigh, and W. K. Hall, *J. Phys. Chem.* **92**, 803 (1988). (b) R. Pis Diez and A. H. Jubert, *J. Mol. Struct. (Theochem)* **210**, 329 (1990). (c) R. Pis Diez and A. H. Jubert, *J. Mol. Catal.* **73**, 65 (1992). (d) M. Neurock and R. A. van Santen, *J. Am. Chem. Soc.* **116**, 4427 (1994).